Available online www.jsaer.com

***Journal of Scientific and Engineering Research*, 2023, 10(4):16-27**

Research Article

ISSN: 2394-2630
CODEN(USA): JSERBR

Numerical Simulation of Vortex-Induced Vibration Dependence on Geometry for Hydrokinetic Energy Converter

Kombo Theophilus-Johnson[1]*, Samuel O. Enibe[2], Chigbo A. Mgbemene[2]

[1]Department of Marine Engineering, Faculty of Engineering, Rivers State University, Nkpolu-Oroworukwo, Port Harcourt, Rivers State, Nigeria.
[2]Department of Mechanical Engineering, Faculty of Engineering, University of Nigeria, Nsukka, Enugu State, Nigeria.
Corresponding Author: Kombo Theophilus-Johnson, Department of Marine Engineering, Rivers State University. Email: kombo.theophilus-johnson@ust.edu.ng

Abstract Flows around oscillating cylinders (circular and rectangular cross-sections) were simulated numerically. This study aims to simulate the potential that exists to harness Vortex-induced vibration (VIV) for electrical energy generation from low velocity marine currents by creating a computer model and exporting it to ANSYS fluent for fluid-structure interaction simulation. The simulation condition was initialized to t = 0, with a time step size of 0.01s, number of time steps was 500 and maximum iteration /time step of 50. Numerical development was performed using ANSYS and MATLAB simulations in which data were sampled at a frequency of 100 Hz. One – degree of freedom mathematical equation of motion models for the heaving bluff body was developed to predict the dynamic response of the cylinders subjected to a range of flow velocities. Responses from the simulations showed variations in the heaving amplitude, vortex-induced vibration aquatic clean energy (VIVACE) power with respect to the geometries and current velocities. Simulation results showed good agreement with literature. A maximum heaving force amplitude and VIVACE power of 30 N and 9.245 kW, and 28 N and 0.799 kW were developed at a current velocity of 1.8 m/s and 100 mm diameter for the rectangular and circular bluff bodies, respectively. Significantly, results of the energy efficiencies showed that the power generation strongly depends on the shape of the cylinder. The rectangular cylinder was found to generate more power than the circular cylinder under the same initial flow conditions.

Keywords Heaving Force Amplitude; Bluff Body; Vortex-induced Vibration; Simulation Condition; Dynamic Response

1. Introduction

Flow around cylinders has been the topic of numerous experimental and numerical investigations because of its significance in engineering projects [1]. Circular and square (or rectangular) cylinders are widely used in mechanical, civil, and naval engineering in such structures as offshore/onshore platforms, power lines, bridge piers, and heat exchangers (chimneys) [1].

The flow around cylinders exhibits numerous important physical phenomena, such as flow separation, vortex shedding, and turbulence. Numerous practical interest in fluid mechanical properties, including drag and lift forces, and pressure coefficients from instigated forces, are significantly influenced by the vortex shedding and suppression mechanism [2]. Studies have shown that continuous use of fossil fuels is not sustainable, pollutes the environment, and causes depletion of the earth's natural resources. Switching from the dependence on fossil fuels will require development of alternative sources of energy that are clean, environmentally friendly, and non-polluting [3]. Tidal streams and ocean current energy are possible renewable sources to provide the required

alternative for the replacement of the fossil fuels [4]. Oceans have a vast and largely untapped resource of energy in motion and has the potential of providing substantial amount of renewable energy, which can be harnessed to generate electricity to power homes, ships, and industries [5].

Several potentially viable ocean-based alternative energy conversion technologies that do not rely on fossil fuels and directly produce any emissions are now available such as the Vortex-induced vibration aquatic clean energy (VIVACE) converter [6]. The VIVACE converter uses the physical phenomenon of Vortex Induced Vibrations (VIV). For this device, enhancing VIV is an important consideration for the extraction of more hydrokinetic energy from fluid flows [6]. There are three very important characteristics that can effectively describe and quantify VIV and they are; amplitude, frequency, and vorticity distribution [6]. VIV is mostly considered as destructive to both equipment and structures, especially causing hydrodynamic excitation that may seriously affect the structural integrity or reliability of performance [7, 8]. Bernitsas and Raghavan in 2005 [9] took an opposite view and tried to maximize VIV, and then found a way to extract the useful energy from the surrounding flow from the oscillatory motion of the cylinder.

The use of VIVACE converter can be employed to solve the problem of electricity generation and eliminates the harmful emissions from greenhouse gases from the use of fossil fuels in coastal communities. Electricity supply to these areas is mostly difficult to achieve due to setbacks such as high cost of utility grid extension where population is separated by the ocean. It has been identified that the Atlantic Ocean for instance possess the conditions necessary to create amplified motion required to support a technically feasible VIVACE converter to generate required power [10]. The VIVACE module can range in size from single cylinder arrays to several-cylinder, mega-watt producing power plant [11].

In this work, we are interested in simulating the effect of the cylinder diameter in enhancing vortex induced vibrations to produce electrical power from the self-sustained oscillations of the hydrokinetic energy converter resulting from this fluttering instability. The device works by securing horizontally a cylinder with elastic springs in flowing water and limiting it to a single degree of freedom, allowing it to oscillate up and down perpendicular to the water current flow [12].

2. The VIVACE Physical Model

A simple schematic of a single physical model of the VIVACE converter considered in this work is shown in Figure2.1. The model consists of a rigid bluff body of diameter *D* and length *L*, two supporting linear springs, two vertical shafts with linear bearings. The rectangular cylinder mounted with its axis in the *z*-direction (horizontally) is to be submerged into the towing tank perpendicularly to the flow velocity *U*, which is in the *x*-direction and will oscillate in the *y*-direction on the vertical shafts using linear bearings perpendicular to its axis in *z* and the *U* velocity in *x*.

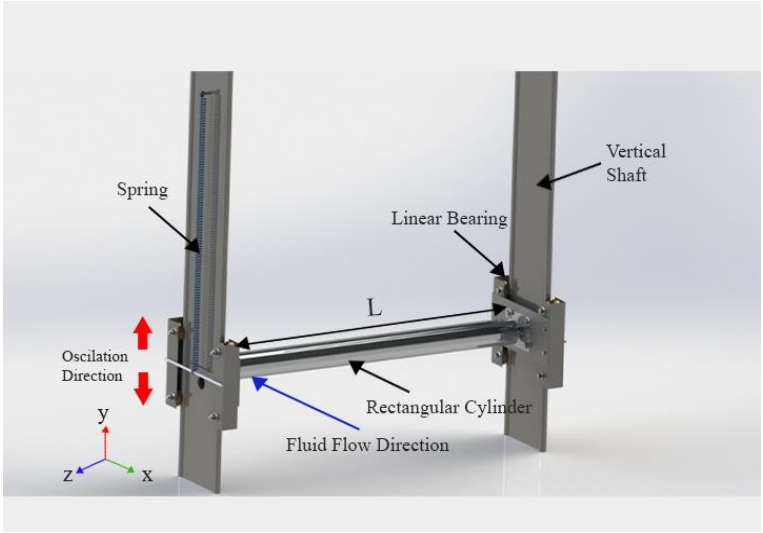

Figure 2.1: Simple schematic model of a rectangular prism VIVACE module

The bluff body is elastically supported by a linear spring and its motion is constrained along the crossflow direction, thus allowing it to move with one-degree of freedom. When the water flow passes the cylinder, it induces periodic drag and lift forces along the surface of the cylinder. This causes vortex shedding on two sides of the wake region behind the cylinder. The cylinder vibrates and oscillates under the influence of lift forces and the constrained restoring spring forces in the crossflow direction. The cylinder vibrations are known as VIV. Each cylinder is connected to a mechanism that converts the VIV into rotational motion of the generator shaft. The shaft motion is subsequently converted to useable energy via appropriate transducers. It is assumed that the VIV of the one-degree-freedom rectangular cylinder approximates the maximum response at resonance.

2.1. Model Setup

The computational domain and the boundary conditions for the simulation of the flow around cylinders are shown in Figure 2.2. Longitudinal uniform velocities varying from 0.513 m/s – 2.565 m/s were introduced at the inlet of the flume, the computational domain, and the boundary conditions for the simulation of the flow around circular and square cylinders shown in Figure 2.3.

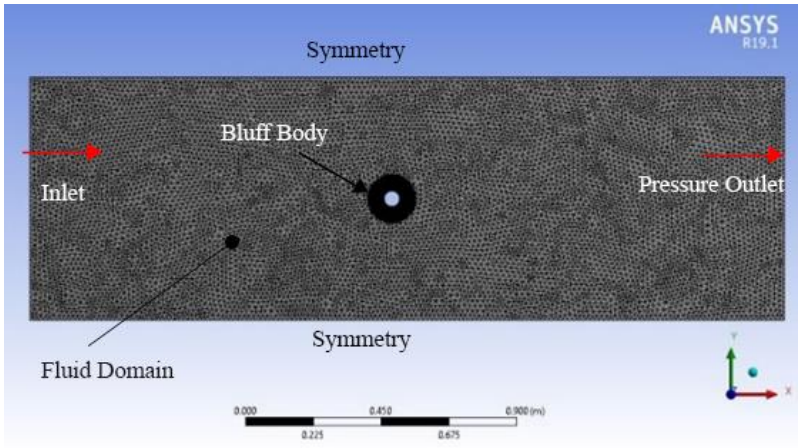

Figure 2.2: Meshed flow domain showing geometry of the model and quality of mesh

Table 2.1: Location of body within the computational domain

Parameters	Dimensions (mm)
D1	50
H3	2500
H5	500
V2	1750
V4	1000

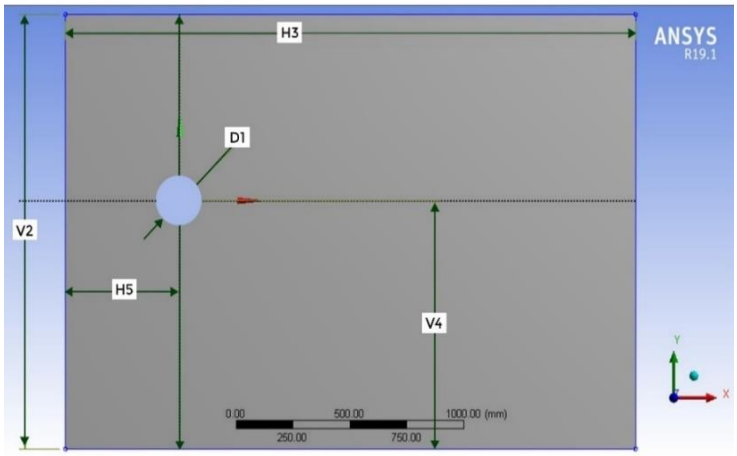

Figure 2.3: Sketch definition of position of the body within the computational domain

Outlet boundary of the channel is defined to be the pressure outlet, with an average reference (gauge) pressure of 0 Pa. The left- and the right-hand side walls of the flume and the cylinder walls have a no-slip boundary condition, where flow velocity is zero at the wall surfaces and increases to the free-stream velocity away from the boundaries. Table 2.1 provides all flow conditions used in the analyses of the flow field associated with different fluid velocity.

The optimum mesh size was selected by a mesh independence study. In that study, the mesh consisted of proximity and curvature; the size of the grid cells affects the outcome of the simulation. The mesh cells used in this research were refined in order to resolve the boundary layer separation and the wake behind the cylinders in the form of the vortex street. Meshing is one of the most important steps in obtaining an accurate boundary layer solution as shown in Figure 2.3 the meshed flow domain showing the geometry of the model and the quality of the mesh used for the cylinder.

3. Preliminary Estimation and Theoretical Development of VIVACE Energy Converter

3.1 Mathematical model

Equation of motion

Consider a cylinder completely immersed horizontally in a fluid of length L and diameter D, as shown in Figure 3.1.

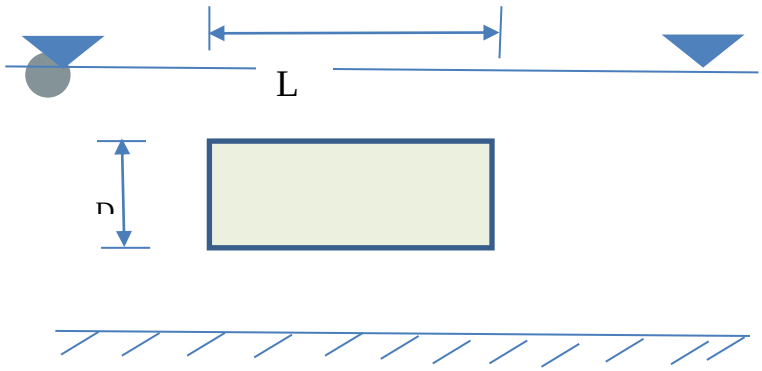

Figure 3.1: A cylinder completely submerged in a fluid

When the body is excited say vertically, and set into motion, the motion equation can be represented mathematically using Newton's law as

$$ma = F \quad (3.1)$$

Where: m = mass of the oscillating body
a = acceleration of the body
F= exciting force.

As the body undergoes oscillations and dampens with time, the motion can best be described using the mass spring damper system since the body carries with it a certain virtual mass of the fluid during the motion. The added mass is the component of the virtual mass resulting from the accelerating motion of the radiating water away from the body, and it also creates a damping effect called radiation or hydrodynamic damping. Again, a restoring force brings the body back to its equilibrium condition. With the analogy of the mass spring damper system and following from equation (3.1), the new equation of motion can be written as

$$(m + A)\ddot{y} + B\dot{y} + Cy = F \quad (3.2)$$

Where: A =added mass of the fluid
B = damping force
C = Restoring coefficient
F = excitation force

The motion equation is a second-order differential equation. The added mass and damping coefficient are hydrodynamic problems that could be solved in a variety of ways. Amongst these methods are the strip and panel methods.

The solution adopted for solving the diffraction problem of the hydrodynamic potentials for this research is the one used by [13]. Here the method of variable separation and Eigen-function expansion is employed. A

vertically fixed submerged cylinder under wave action in finite water depth d is considered, as shown in Figure 3.1.

To solve the modified equation of motion according to equations (3.3) and (3.4), having obtained the values of b_{33} and m_{a33} from the multipole method,

$$(m_s + m_{a33})\ddot{y} + b_{33}\dot{y} + (c_{33} + k_{33})\, y = F_L * sin(\omega_s t + \varphi) \quad (3.3)$$

For a fully submerged cylinder, there is no free water plane area making the hydrostatic restoring capability (c_{33}) to be zero and thus the only restoring force comes from the external stiffness (k) offered by the springs. The final equation of motion to be solved is thus represented according to equation (3.4)

$$(m_s + m_{a33})\ddot{y} + b_{33}\dot{y} + k_{33}y = F_L * sin(\omega_s t + \varphi) \quad (3.4)$$

The use of the state space method is deployed, where the second-order equation of motion is disintegrated into two first-order equations and solved using Runge-Kutta-Fehlberge (RKF45) and Adams predictor /corrector formula method.

The state-space method is used to decompose the resulting 2nd-order ordinary differential equation (ODE) into two sets of 1st ODE and solved concurrently.

Linear equations for the amplitude of oscillations and lift coefficient are given as

$$y(t) = y_{max} \sin(2\pi f_s t) \quad (3.5)$$

$$c_{L(t)} = C_L * \sin(\omega t + \varphi) \quad (3.6)$$

$$c_L(t) = C_L \sin(2\pi f_s t + \varphi) \quad (3.7)$$

Where: y_{max} = maximum amplitude of oscillation

φ = phase angle between fluid force and displacement

c_L = time independent lift coefficient

C_L = amplitude of lift coefficient of the cylinder

The power in the fluid flowing over the cylinder whose motion is perpendicular to the fluid flow is given as

$$F_L = \frac{1}{2}\rho U^2 \text{ x } DL * C_L \quad (3.8)$$

$$F_L(t) = F_L * \sin(2\pi f_s t + \varphi) \quad (3.9)$$

$$F_L(t) = \frac{1}{2}\rho U^2 * DL * c_L(t) \quad (3.10)$$

Where: F_L = power in the fluid

ρ = density of the fluid

D = characteristic dimension of the cylinder in the direction transverse to the incident flow

L = length of the cylinder

Note that; DL is the projected area in the direction perpendicular to fluid flow available for the dynamic pressure to develop the fluid force.

Work done by the fluid acting on the bluff body during a VIV cycle is given by

$$W_{VIVACE} = \int_0^{T_{cyl}} F_{fluid}\, \dot{y} dt \quad (3.11)$$

$\dot{y}$ Represents the oscillation velocity in this case, the heave velocity of the oscillating cylinder.

The fluid power due to VIV is

$$P_{VIVACE} = \frac{W_{VIVACE}}{T_{cyl}} \quad (3.12)$$

The fluid power P_{VIVACE} from VIVACE due to VIV can be obtained by multiplying the force from equation (3.2) by the instantaneous velocity and integrating it to obtain

$$P_{VIVACE} = \frac{1}{2}\rho\pi U^2 C_L f_s y_{max} DL sin(\varphi) \quad (3.13)$$

The efficiency of the system can be given as

$$\eta_{VIVACE} = \frac{P_{VIVACE}}{Power\ in\ the\ fluid} \quad (3.14)$$

From equations (10) and (13)

$$\eta_{VIVACE} = \frac{\frac{1}{2}\rho\pi U^2 C_L f_s y_{max} DL sin(\varphi)}{\frac{1}{2}\rho U^2 * DL * c_L} \quad (3.15)$$

Computational Results

Computation was carried out for series of flows around the cylinders with circular and rectangular cross-sections subjected to transverse oscillations in a uniform flow. The results of the oscillating cylinder are presented here. Figures 3.1 to 3.6 show (a) velocity contours, and (b) oscillatory lift force, respectively.

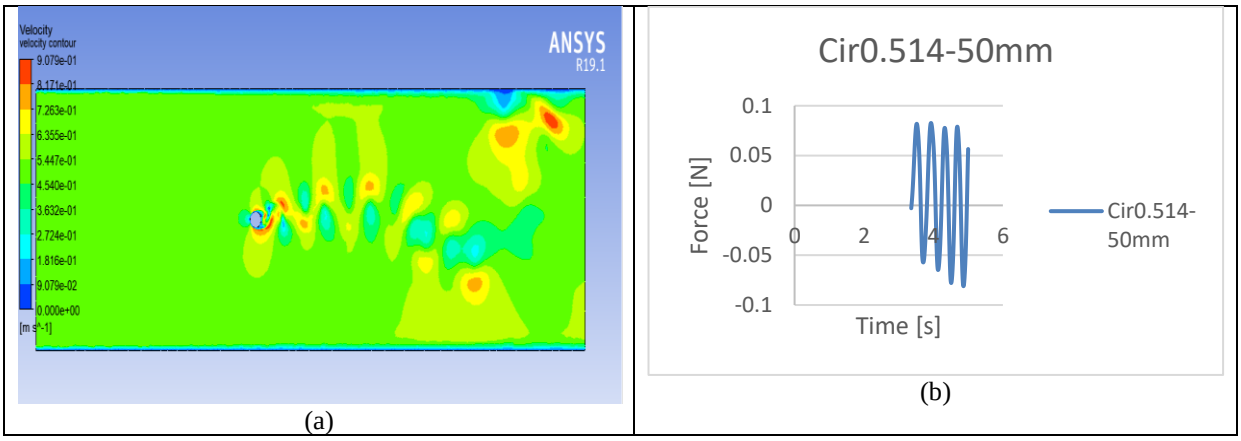

(a) (b)

Figure 3.1: Results of circular cylinder of diameter 50mm and velocity 0.514m/s oscillating transversely

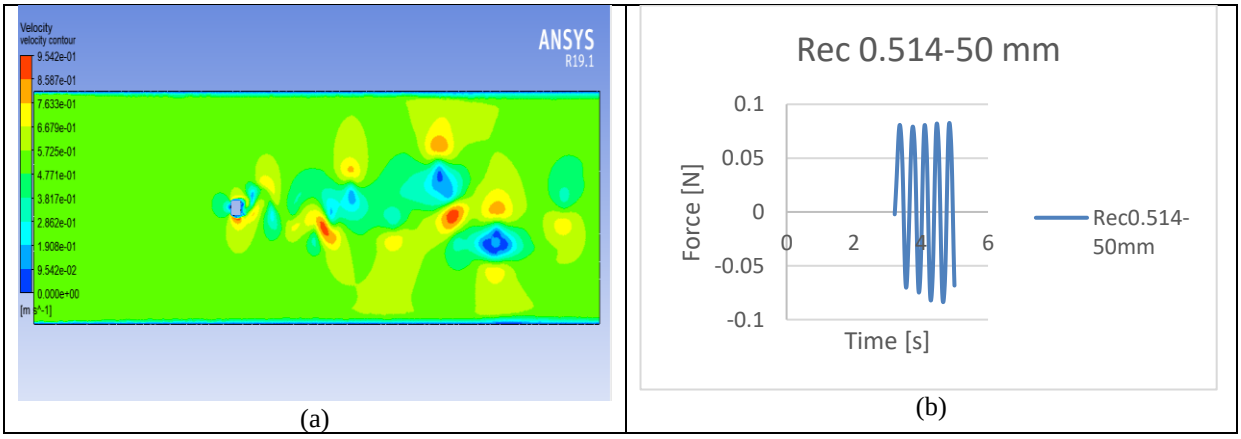

(a) (b)

Figure 3.2: Results of rectangular cylinder of diameter 50mm and velocity 0.514m/s oscillating transversely

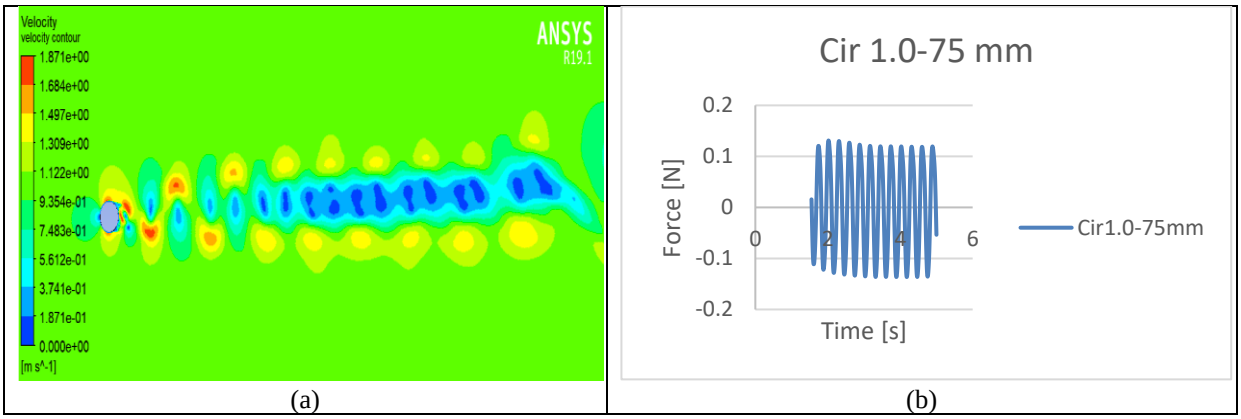

(a) (b)

Figure 3.3: Results of circular cylinder of diameter 75mm and velocity 1.0m/s oscillating transversely

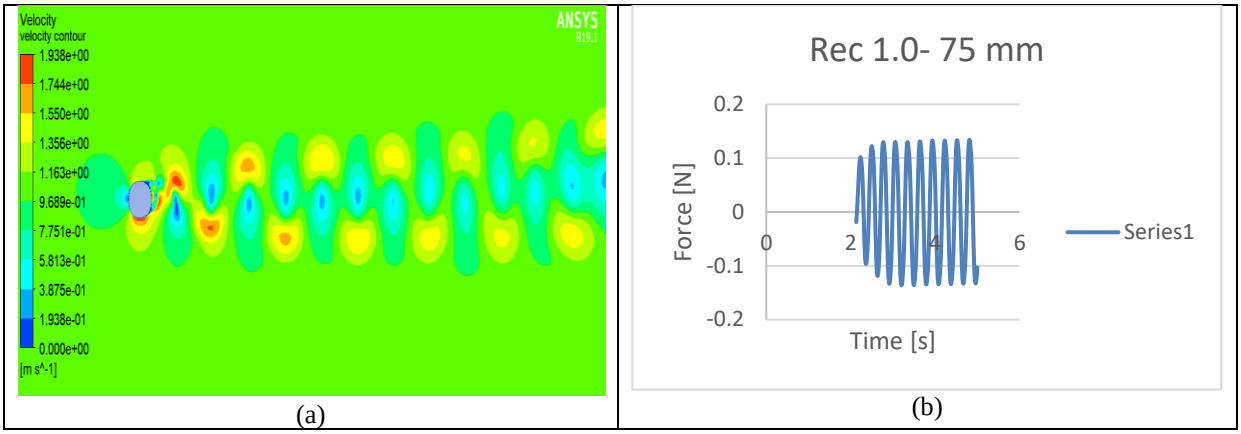

(a) (b)

Figure 3.4: Result of rectangular cylinder of diameter 75mm and velocity 1.0m/s oscillating transversely

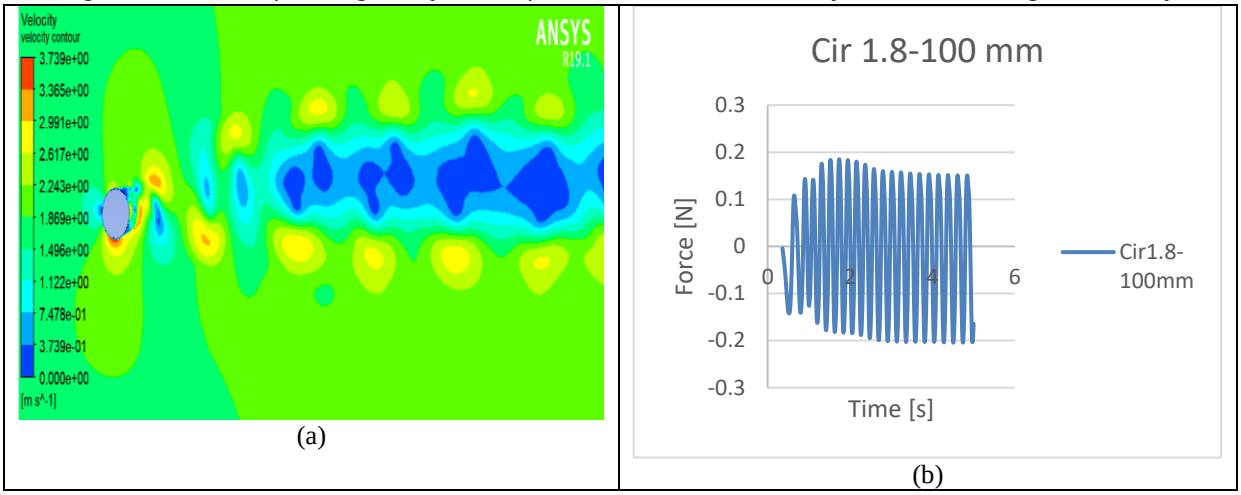

(a) (b)

Figure 3.5: Result of circular cylinder of diameter 75mm and velocity 1.8m/s oscillating transversely

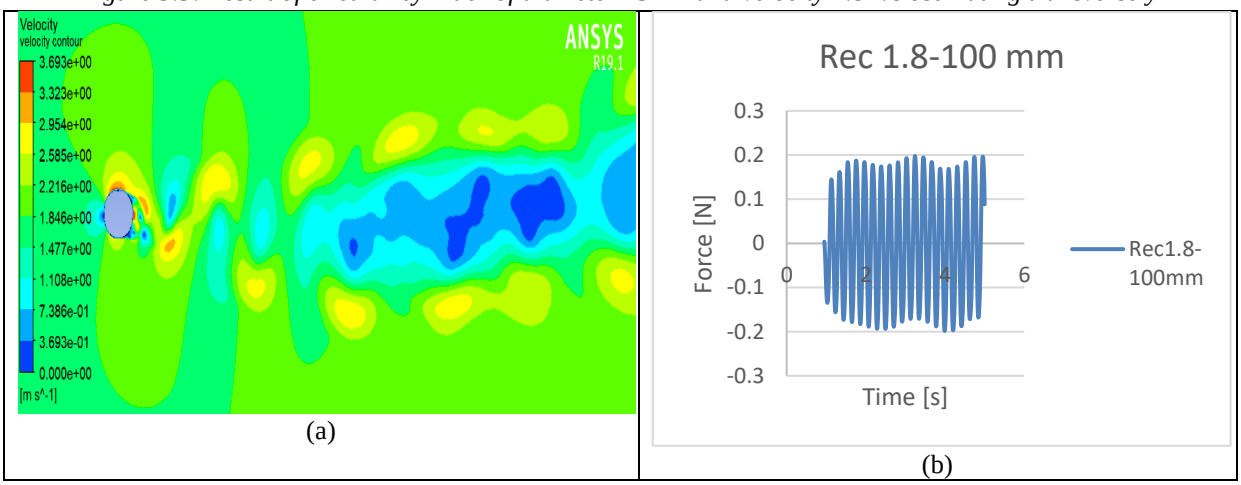

(a) (b)

Figure 3.6: Result of rectangular cylinder of diameter 100mm and velocity 1.8m/s oscillating transversely

It is observed in Figure 3.1a that the flow pattern over the front and back are quite different. The flow smoothly passes the cylinder in the front but in the wake, the flow is unsteady, and vortices are shed downstream. There are no large cross-stream oscillations in the cylinder position which may be attributed to no coupling of the frequency to the natural frequency of the cylinder. It is observed further downstream that the vortices formed in the wake gradually die down. Figure 3.1b shows plot of the oscillatory force acting on a circular cylinder against the time of oscillation of the body at a velocity of 0.514 m/s. The body maintains a steady oscillatory motion as

the time of oscillation increased from a period of 0s to 1.64 s. As the period of oscillation increases, the force keeps increasing and decreasing at varying time intervals.

Figure 3.2a show the flow past a rectangular cylinder of diameter 50mm and 0.514m/s flow velocity. It is observed that the flow is somewhat different compared to that of the circular cylinder at same velocities. The vortices die down slower further downstream. Separation occurs much quicker as a result of the corners of the cylinder. The vortices formed at the corners are slightly attached or slightly interactive. The net pressure produced would move the body upwards thereby producing a crossflow response. No noticeable large cross-stream oscillations in the cylinder position. Figure 3.2b shows the graph of the force acting on the rectangular bluff body of 50 mm diameter against the period of oscillation of the body at a velocity of 0.514 m/s. The force acting on the rectangular bluff body increased as the period of oscillation increased from 0 s to 0.15 s, respectively. The plot follows a sinusoidal wave pattern repeatedly as the period continuous to increase.

Figure 3.3a and 3.4a show a lower distorted flow field in the wake compared to previous cases, 0.514 m/s and 0.7 m/s flow fields. The increasing inlet flow velocity may be responsible for this wake pattern. It shows that the flow frequency gradually decouples from the natural frequency of the cylinders thereby causing a no large cross-stream oscillations in the cylinder position. Vortices are broken down much faster in the case of the rectangular cylinder (3.4a). Figure 3.2b shows the graph of the force acting on the circular cylindrical body of diameter 75 mm against the period of oscillation at a velocity of 1.0 m/s. The force acting on the cylinder dropped suddenly as the period of oscillation increased from 0 s to 0.06 s, respectively. The force on the body later increased as the period of oscillation increased from 0.06 s to 0.19 s respectively. The process formed a sinusoidal wave pattern repeatedly as the period of oscillation increased from 0s to 3.45 s. Figure 8b shows the graph of the force acting on the rectangular bluff body of 75 mm diameter against the period of oscillation of the body at a velocity of 1m/s. The force acting on the rectangular bluff body increased as the period of oscillation increased from 0 s to 0.1 s, respectively. At this point, the force action on the body dropped sharply and later increased as the period of oscillation increased to 0.37 s. The oscillation procedure was repeated for up to a period of 2.87 s forming a sinusoidal wave pattern.

At 1.8 m/s inlet velocity, it was observed in Figure 3.5a and Figure 3.6a that there is a large area of pressure field around the stagnation points of both cylinders. Both cylinders have almost identical wake regions. Vortices are formed around both cylinders and are attached. In Figure 3.5b the force acting on the cylinder dropped suddenly as the period of oscillation increased from 0 s to 0.16 s, respectively. As the period of oscillation increased from 0.29s to 0.44 s, the force acting on the cylinder decreased. The oscillation process of the circular cylinder continued to fluctuate up and down forming a sinusoidal wave pattern as the period of oscillation increased from 0s to 4.46 s. Figure 10b shows that the force acting on the bluff body decreased sharply as the period of oscillation increased from 0s to 0.08 s, respectively. This process also formed a sinusoidal wave pattern as the period of oscillation increased up to 4.05s.

Table shows the optimized heave force F_L for three cases of circular and rectangular bluff bodies calculated using equation (10). From the graph of heave force amplitude and current velocity shown in Figure3.7, the maximum heaving force amplitude of 30 N emanates from the rectangular cylinder of 100 mm diameter followed by that of the circular cylinder of the same diameter which indicated a heaving force of 28 N at current velocity of 1.8 m/s. This signifies a 6.67 % fall in the heave force which is due to the reduction in the vortex effect from the sharper rectangular edge compared to the circular surface.

Table 3.1: Optimized heave force amplitude for different cases of bluff bodies using sum of sine fit in MATLAB Cftool.

Case	Velocity (m/s)	DL (m^2)	$\rho\ kg/m^3$	C_L (-)	F_L (N)
Cir0.514-50mm	0.514	0.05	995.6	0.07018	0.46149
Cir1.0-75mm	1	0.075	995.6	0.1301	4.85728
Cir1.8-100mm	1.8	0.1	995.6	0.1716	27.6769
Rect0.514-50mm	0.514	0.05	995.6	0.07888	0.5187
Rect1.0-75mm	1	0.75	995.6	0.131	4.89089
Rect1.8-100mm	1.8	0.1	995.6	0.1862	30.0317

Similarly, at current velocity of 1.8 m/s, the circular and rectangular cylinders of 50 mm diameter recorded a heaving force of 4.1 N and 4.9 N, respectively. The heaving force amplitude for the 75 mm diameter circular and rectangular cylinders seem to overlap but as the flow velocity increases, the rectangular cylinder showed a higher heaving force amplitude than the circular cylinder. From the foregoing, it can be deduced that the rectangular cylinder gives the highest heaving force amplitude of oscillation of 30 N.

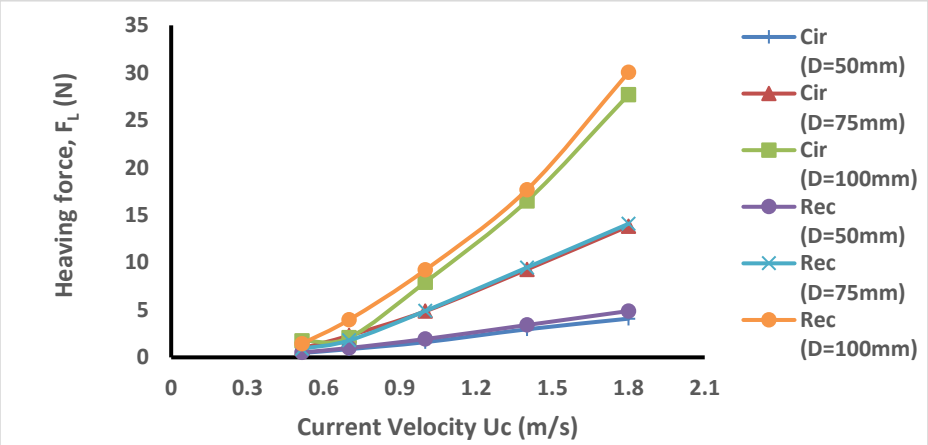

Figure 3.7: Plot of heaving force amplitude vs velocity

4. Conclusion

In this paper, the effect of geometry has been shown to have positive impact in the generation of energy from VIV through the use of CFD with rectangular and circular geometries. Computational studies carried out shows that the rectangular profile VIVACE converter extracts energy successfully and efficiently from fluid flow than its equivalent circular profile.

The velocity contour plots from the CFD analysis gave useful results showing that a net pressure exists which would make the cylinder move upwards thereby producing a crossflow response. This crossflow response could be termed as the lift experienced by the cylinder and a wake pattern just immediately after the bluff body. Results of analysis carried out show that the current, shape and size or diameter of the body affects the amplitude of the heave disturbance or response. This in turn directly affects the power that can be generated by the VIVACE. VIVACE power of 9.245 kW and 0.799 kW at 1.8 m/s were achieved with the 100 mm rectangular and circular bluff bodies, respectively.

References

[1]. A. Okajima, K. Kitajima, and H. Ueno, "Numerical Study on Wake patterns and Aerodynamic Forces of an Oscillating Cylinder with a Circular and Rectangular Cross-section," *Journal of Wind Engineering and Industrial Aerodynamics, Elsevier Science Publishers*, vol. 50, no. 1993, pp. 39 - 48, 1993.

[2]. A. M. Bimbato, L. A. A. Pererira, and M. H. Hirata, "Study of the Vortex Flow around a Body Near a Moving Ground," *Journal of Wind Engineering and Industrial Aerodynamics*, vol. 99, no. 1, pp. 7-17, 2011, doi: 10.1016/j.jweia.2010.10.003.

[3]. Beachapedia. "Renewable Ocean Energy." www.beapedia.org/Renewable_Ocean_Energy (accessed.
[4]. S. Omer, "Numerical Assessments of Ocean Energy Extraction from Western Boundary Currents using Quasi-Geostrophic Ocean Circulation Model," *International Journal of Marine Energy*, vol. 36, no. 2016, pp. 12 - 29, 2016.
[5]. Wikipedia. "Marine Energy." https://en.m.wikipedia.org/wiki/marine_energy (accessed.
[6]. L. Ding, L. Zhang, C. Wu, X. Mao, and D. Jiang, "Flow Induced Motion and Energy Harvesting of Bluff Bodies with Different Cross-Sections " *Journal of Energy Conversion and Management*, vol. 91, pp. 416-426, 2015, doi: 10.1016.2014.12.039.
[7]. I. Ball, T. Killen, S. Sakhuja, and E. Warner, "Maximizing Vortex Induced Vibrations Through Geometry Variation," Bachelor of Science Project, Mechanical Engineering, Worchester Politechnic Institute, Massachusetts, United States of America BJSF011, 2012.
[8]. M. M. Bernitsas, K. Raghavan, Y. Ben-Simon, and E. M. H. Garcia, "VIVACE (vortex induced vibration aquatic clean energy): A New Concept in Generation of Clean and Renewable Energy from Fluid Flow," *Journal of Offshore Mechanics and Arctic Engineering – Transactions of the ASME*, vol. 130, no. 4, pp. 041101-15, 2008.
[9]. M. M. Bernitsas and K. Raghavan, "Fluid Motion Energy Converter," United State Patent 11/272504, 2005a.
[10]. K. Theophilus-Johnson, S. O. Enibe, and C. A. Mgbemene, "Extracting Ocean Energy for Electricity Generation," in *5th High-Level Industry, Science and Government Dialogue on Atlantic Interaction*, Lagos, Nigeria, 2019: Atlantic International Research Center.
[11]. A. Hall-Stinson, C. Lehrman, and E. Tripp, "Energy Generation from Vortex Induced Vibrations," Bachelor of Science Projet, Mechanical Engineering, Worcester Polytechnic Institute, Massachusetts, United States of America, BIS-VE10, 2011. [Online]. Available: https://web.wpi.edu
[12]. K. Raghavan, "Energy Extraction from a Steady Flow Using Vortex Induced Vibrations," Ph.D. Dissertation, Naval Architecture and Marine Engineering, University of Michigan, Michigan, United States of America, 2007.
[13]. J. Sheng-Chao, Ying, G., and Bin, T., "Water Wave Radiation Problem by a Submerged Cylinder," *Journal of Engineering Mechanics*, vol. 140, no. 5, p. 13, 2014, doi: 10.1061/CASCE/Em, 1943-7889.0000723.

Appendix

Cylinder Type	Cylinder Size	Fluid Inlet Velocity (Knots)	Average Velocity [m s^-1]	Displacement (m)	Acceleration [m s^-2]	Max Flow Velocity [m s^-1]
Rectangle	50mm	1	0.511657	2.558	0.071212	0.960988
		1.8	0.925256	4.62628	0.0766495	1.74074
		2.6	1.33037	6.65185	0.130276	2.4331
		3.4	1.74792	8.7396	0.0831657	3.41625
		4.2	2.15563	10.7782	0.101064	3.86601
		5.0	2.53425	12.6713	0.0382318	4.90487
		5.8	2.95175	14.7587	0.445197	6.10599
Circular	50mm	1	0.522106	2.61053	0.0273605	0.924335
		1.8	0.939867	4.69934	0.117348	1.7284
		2.6	1.36197	6.80985	0.0556334	2.46192
		3.4	1.76917	8.84585	0.15572	3.04854
		4.2	2.16009	10.8004	0.264553	3.87521
		5.0	2.54249	12.7125	0.365975	4.37535
		5.8	2.93167	14.6583	0.427881	5.04804
Rectangle	70mm	1	0.519735	2.59867	0.0433692	0.950854
		1.8	0.946718	4.73359	0.0562129	1.99847
		2.6	1.37195	6.85975	0.0741981	2.95666
		3.4	1.78186	8.9093	0.219675	3.56568
		4.2	2.1969	10.9845	0.0795357	4.34812
		5.0	2.61724	13.0862	0.131726	4.78915
		5.8	3.04585	15.2292	0.103332	5.94769
Circular	70mm	1	0.528446	2.64223	0.0665254	0.984738
		1.8	0.961616	4.80808	0.106633	1.77806
		2.6	1.38464	6.9232	0.147127	2.65833
		3.4	1.80808	9.0404	0.0517424	3.38532
		4.2	2.18879	10.944	0.112267	3.7646
		5.0	2.60781	13.0391	0.373197	4.64114
		5.8	3.04333	15.2167	0.159726	5.4612
Rectangle	90mm	1	0.528163	2.64082	0.135582	1.38908
		1.8	0.951799	4.759	0.108014	1.89511

		2.6	1.37353	6.86764	0.155439	3.07349
		3.4	1.80936	9.04678	0.0247222	3.80588
		4.2	2.21328	11.0664	0.181264	4.03064
		5.0	2.66414	13.3207	0.134957	5.6056
		5.8	3.0876	15.438	0.250633	6.80938
		1	0.527278	2.63639	0.031737	0.995365
		1.8	0.965602	4.82801	0.0881194	1.76251
		2.6	1.38786	6.9393	0.143873	2.51368
Cylinder	90mm	3.4	1.80021	9.00105	0.106619	3.23021
		4.2	2.20872	11.0436	0.321819	4.23799
		5.0	2.61974	13.0987	0.444234	5.00869
		5.8	3.03524	15.1762	0.18785	5.72114
		1	0.537419	2.68709	0.0711838	1.35613
		1.8	0.954383	4.77191	0.109186	1.97579
		2.6	1.36867	6.84336	0.0637962	2.75027
Rectangle	100mm	3.4	1.80437	9.02185	0.224372	3.85981
		4.2	2.2591	11.2955	0.184288	4.63852
		5.0	2.65629	13.2815	0.309854	5.85133
		5.8	3.06185	15.3092	0.167896	6.14508
		1	0.539324	2.69662	0.0333094	1.23548
		1.8	0.964201	4.821	0.115003	2.09509
		2.6	1.40661	7.03305	0.00578489	2.70642
Cylinder	100mm	3.4	1.83546	9.17729	0.124843	3.40995
		4.2	2.26423	11.3211	0.169964	4.10224
		5.0	2.65888	13.2944	0.152904	5.11777
		5.8	3.07654	15.3827	0.185989	5.95144